

## Navigating Localized Wave Packets in Phase Space

W. Zhao,<sup>1</sup> J. J. Mestayer,<sup>1</sup> J. C. Lancaster,<sup>1</sup> F. B. Dunning,<sup>1</sup> C. O. Reinhold,<sup>2,3</sup> S. Yoshida,<sup>4</sup> and J. Burgdörfer<sup>4,3</sup>

<sup>1</sup>*Department of Physics and Astronomy and the Rice Quantum Institute, Rice University, Houston, Texas 77005-1892, USA*

<sup>2</sup>*Physics Division, Oak Ridge National Laboratory, Oak Ridge, Tennessee 37831-6372, USA*

<sup>3</sup>*Department of Physics, University of Tennessee, Knoxville, Tennessee 37996-1200, USA*

<sup>4</sup>*Institute for Theoretical Physics, Vienna University of Technology, Vienna, Austria*

(Received 29 June 2006; published 20 December 2006)

The ability to localize and to steer Rydberg wave packets in phase space using tailored sequences of half-cycle pulses is demonstrated. Classical phase-space portraits are used to explain the method and to illustrate the level of control that can be achieved. This is confirmed experimentally by positioning a phase-space-localized wave packet at the center of a stable island or navigating it around its periphery. This work provides a valuable starting point for further engineering of electronic wave functions.

DOI: 10.1103/PhysRevLett.97.253003

PACS numbers: 32.80.Rm, 32.60.+i, 32.80.Qk

Atoms in high-lying Rydberg states with large values of principal quantum number  $n$  provide a valuable laboratory in which to explore control of the quantum states of mesoscopic systems [1–4]. Such atoms can be manipulated using one or more pulsed unidirectional electric fields, termed half-cycle pulses (HCPs), of duration  $T_p \ll T_n$ , where  $T_n$  is the classical Kepler orbital period. In this limit, each HCP,  $F_{\text{HCP}}(t)$ , delivers an impulsive momentum transfer or “kick”  $\Delta p = -\int F_{\text{HCP}}(t)dt$  to the excited electron [5]. (Unless otherwise specified, atomic units are used throughout.)

A remarkable degree of control over Rydberg wave packets can be achieved using HCP trains [6]. The underlying classical phase space features stable islands surrounded by a chaotic sea. Placing a wave packet in a stable island gives rise to “dynamical stabilization,” i.e., to creation of a nondispersive wave packet [7]. Conversely, placing a wave packet in the chaotic sea results in rapid spreading and, eventually, in ionization. Rydberg wave packets can, in principle, be “steered” to different regions of phase space, i.e., regions of coordinate and momentum space, and even focused, by adiabatically chirping the amplitude and/or frequency of the HCP train [6]. Furthermore, by sudden changes in the HCP amplitude or frequency the wave packet can be switched from one island to another. A critical first step is the production of a wave packet that is strongly localized within an island. We demonstrate here that starting with very high  $n$  quasi-one-dimensional (quasi-1D) Rydberg atoms it is possible to create localized wave packets and position them either near the periphery (the “shore”) of an island or near its center. The ensuing evolution of the wave packet gives rise to periodic transient phase-space localization at locations that can themselves vary periodically with time providing the opportunity for optimal transfer to other islands. (In the following we use the term “wave packet” and “phase-space distribution” interchangeably because on the time scale of the present experiments quantum effects do not play a significant role.) The present protocol for selectively loading an island is remarkably efficient with  $\sim 90\%$  of

the initial quasi-1D Rydberg atoms becoming trapped within it.

The pulse sequence used in the present protocol is depicted in Fig. 1 and comprises two “preparation” pulses, a periodic HCP train that generates the islands of stability into which the wave packet is placed, and a probe pulse used to analyze experimentally the final wave packet. The control parameters employed here are (i) the time delay,  $t_D$ ,

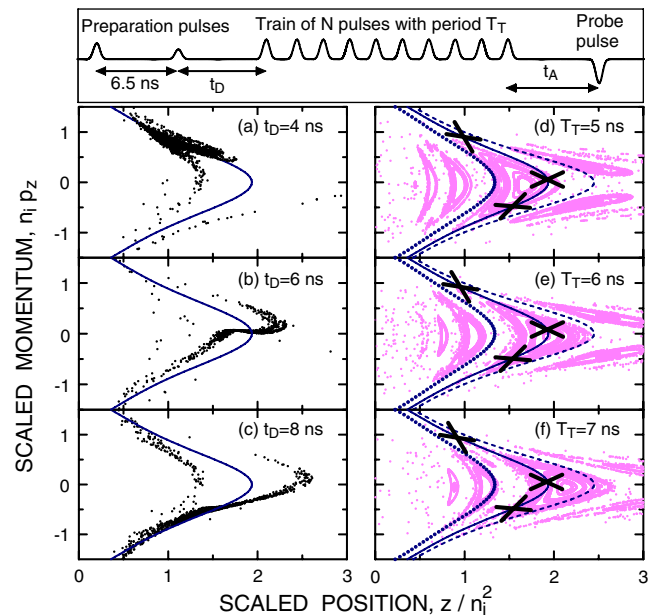


FIG. 1 (color online). Top: Profile  $F(t)$  of applied HCP sequence. (a)–(c) Phase-space portraits of the wave packet following different delay times  $t_D$ . The solid line shows the torus for the unperturbed initial state. (d)–(f) Poincaré surfaces of section for the 3D kicked hydrogen atom and trains of kicks with scaled strength  $\Delta p_0 = -0.1$  and various periods  $T_T$ . The cuts are taken immediately after each kick and correspond to  $\rho_0 \sim 0.5 \pm 0.2$ ,  $p_{\rho_0} \sim 0 \pm 0.2$ . The dashed, solid, and dotted lines show, for a 3D atom, the stationary tori that correspond to scaled energies of  $-0.4$ ,  $-0.5$ , and  $-0.7$ , respectively. The crosses mark the centers of the wave packets shown in (a)–(c).

between the preparation pulses and the HCP train, which controls the initial wave packet location, and (ii) the period,  $T_T$ , of the train, which adjusts the position of the targeted stable island. Other parameters, like the pulse strengths, are kept constant.

Figure 1 illustrates the dynamics underlying the present protocol. We start with potassium atoms photoexcited to a narrow range of the lowest-lying redshifted states in the  $n_i = 350$  Stark manifold. (Because of the Doppler shifts associated with small beam divergences, photoexcitation leads to production of an incoherent mixture of  $\sim 36$  Stark states centered on the parabolic quantum number  $n_1 = 320$  [8], a mix that is used in our simulations.) These quasi-1D states are oriented along the  $+z$  axis (i.e., the  $z$  component of the electric dipole moment  $d = -\langle \Psi | z | \Psi \rangle = -\langle z \rangle$  is negative). The first weak “localizing” HCP provides a kick of scaled strength  $n_i \Delta p_L = -0.085$  directed towards the nucleus. (Note that a HCP applied in the  $+z$  direction delivers a kick to the electron in the  $-z$  direction.) This creates a wave packet that, after a time delay of 6.5 ns ( $\sim T_{n_i}$ ), undergoes strong transient localization into a region of phase space that is smaller than the size of the target island and is located near the outer classical turning point ( $z \sim 2n_i^2$ ) [9] with a mean  $z$  component of momentum  $p_z \sim 0$ . A second HCP with scaled strength  $n_i \Delta p/2 = -0.05$  provides initial “positioning” in momentum space as will be discussed later. Classical trajectory Monte Carlo (CTMC) simulations showing the subsequent evolution of the wave packet are presented in Figs. 1(a)–1(c) for different time delays  $t_D$ . The centers of these wave packets are marked by crosses in Figs. 1(d)–1(f).

Poincaré surfaces of section showing the islands of stability into which the wave packet is loaded are presented in Figs. 1(d)–1(f). These surfaces of section were generated for a hydrogen atom subject to  $\delta$ -function impulses using the Hamiltonian

$$H^{\text{Train}}(t) = H^{\text{at}} + z \Delta p \sum_{k=1}^N \delta(t - kT_T), \quad (1)$$

where the number of applied kicks is  $N$  and  $H^{\text{at}}$  is the atomic Hamiltonian. [In the comparisons with experiment presented below, the dynamics is governed by the Hamiltonian  $H = H^{\text{at}} + zF(t)$  and the actual pulse profile, not  $\delta$ -shaped kicks, are used.] The stroboscopic snapshots used in generating Figs. 1(d)–1(f) were taken immediately *after* each kick. Since each lies on a four-dimensional (4D) manifold, visualization in terms of a surface of section requires reduction to a two-dimensional manifold by slicing the 4D manifold into layers defined [using cylindrical coordinates  $(z, \rho, \phi)$ ] by fixed coordinates  $(\rho \pm \Delta\rho, p_\rho \pm \Delta p_\rho)$ . As this work centers on quasi-1D states, the slice used in Fig. 1 was taken near the center of such states at  $\rho/n_i^2 \sim 0.5$ ,  $n_i p_\rho \sim 0$ , and  $L_z = 0$ .

We focus here on the largest period-one island whose physical origin can be understood by noting that (classically) a kick  $\Delta \vec{p} = \hat{z} \Delta p$  leads to a change in the electron

energy of  $\Delta E = \Delta p^2/2 + p_{zi} \Delta p$ , where  $p_{zi}$  is the initial  $z$  component of electron momentum. For an atom to survive many kicks the electron energy must be little changed following each kick, requiring  $p_{zi} \sim -\Delta p/2$ . After the kick the electron final momentum is  $p_{zf} \sim +\Delta p/2$ . The dominant islands in Fig. 1 are thus centered on  $p_{z_0} = \Delta p_0/2 = -0.05$ . (The second preparation pulse serves to center the wave packet on this value.) Trajectories removed from the center of the stable island follow quasiperiodic orbits and on a surface of section appear to rotate around the central (periodic) orbit. This “rotational” motion is exploited as discussed later. The value of  $T_T$  controls the position of the center of the island with respect to the initial energy manifold (torus) given by  $n_i^2 H^{\text{at}} = -0.5$ . For  $T_T = 5$  ns, corresponding to a scaled frequency  $\nu_0 = \nu_T/\nu_{n_i} = 1.3$ , where  $\nu_T = 1/T_T$  is the kick frequency and  $\nu_{n_i} = 1/T_{n_i}$  is the Kepler frequency, the center of the island is located to the left of the initial torus [Fig. 1(d)]. As  $T_T$  increases, the center moves towards larger values of  $z$  such that for  $T_T = 6$  ns ( $\nu_0 = 1.09$ ) it approximately intersects the initial torus [Fig. 1(e)] whereas for  $T_T = 7$  ns ( $\nu_0 = 0.93$ ) it is situated to the right of the initial torus [Fig. 1(f)].

To highlight the present capabilities we consider selectively placing the wave packet near the shore of the stable island, indicated schematically in Fig. 2. We choose the control parameters  $t_D \sim 4$  ns and  $T_T = 5$  ns. The wave

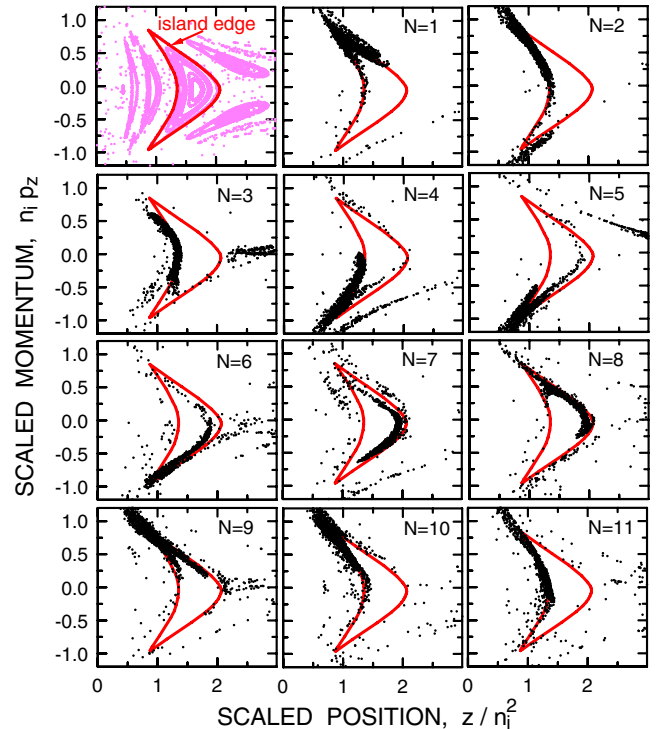


FIG. 2 (color online). Phase-space portraits showing the evolution of the quasi-1D wave packet during the periodic train of kicks for  $T_T = 5$  ns and  $t_D = 4$  ns. The wave packet is selectively placed at the periphery of the main island, denoted by the thick solid line. The corresponding Poincaré surface of section is shown at the top left frame. The cuts are the same as in Fig. 1.

packet circumnavigates the island as the number  $N$  of kicks increases. After  $N = 9$  HCPs the wave packet returns to its starting point with remarkably little dispersion. The motion of the wave packet around the border of the island implies oscillatory behavior in the average electron momentum,  $\langle p_z \rangle$ , as  $N$  increases (see Fig. 3). Since, as noted earlier, the energy transfer,  $\Delta E$ , produced by a HCP, and thus the survival probability, depends on  $p_{zi}$  [10,11], these changes in  $\langle p_z \rangle$  can be seen using a probe HCP applied at a fixed time delay  $t_A (= T_T)$  after the last HCP in the train. As shown in Fig. 3, the measured survival probability undergoes strong oscillations as  $N$  increases that mirror the predicted changes in  $\langle p_z \rangle$ . The results are in reasonable accord with the CTMC simulations, which assume that states with  $n \geq 800$  are ionized by stray residual fields in the apparatus and that there are 10% noise fluctuations in the period and amplitude of the train. The damping of the measured oscillations is somewhat more rapid than predicted, which can be attributed to small field inhomogeneities present in the experimental region.

The present experimental results were obtained using apparatus described in detail elsewhere [12]. Potassium atoms contained in a collimated beam are photoexcited in a weak dc field,  $\sim 250 \mu\text{V cm}^{-1}$ , to low-lying quasi-1D  $n_i = 350$  Stark states using an extracavity-doubled CR699-21 Rh6G dye laser. Experiments are conducted in a pulsed mode. The output of the laser is chopped into a train of pulses of  $\sim 1 \mu\text{s}$  duration using an acousto-optic modulator. Following excitation, the atoms are subject to

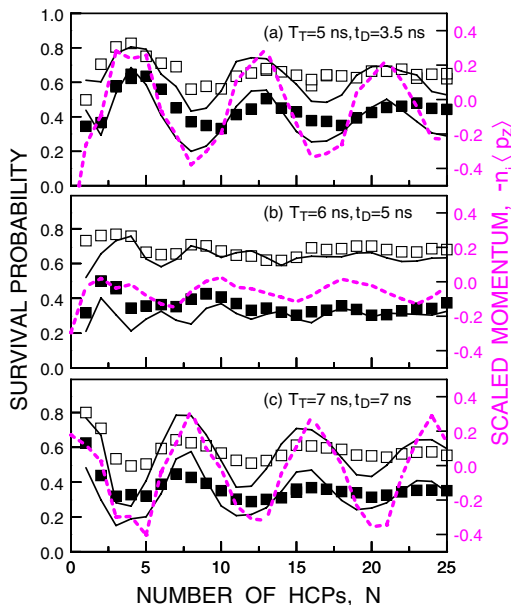


FIG. 3 (color online).  $N$  dependence of the average scaled electron momentum  $n_i \langle p_z \rangle$  (dashed line) and survival probabilities measured using probe pulses of scaled strength  $\Delta p_{A_0} = n_i \Delta p_A = 0.7$  (open squares) and 1.05 (solid squares) for different values of  $T_T$  and  $t_D$ . The solid lines show CTMC simulations that use the experimental pulse profiles (see text).

the HCP sequence (Fig. 1) which was produced by using a combiner to superpose the outputs of several fast pulse generators and applying the resulting waveform to a nearby electrode. The profiles of the applied pulses were measured using a fast probe and storage oscilloscope and typically had durations of  $\sim 600$  ps full width at half maximum. These measurements revealed an artifact associated with the pulse generator used to produce the train of  $N$  HCPs. While the amplitudes and profiles of these pulses were essentially constant, the separation between the first two pulses was systematically 16% larger than that between succeeding pairs of pulses. (This anomaly is included in the simulations.) The number of atoms that survive the HCP sequence is determined using selective field ionization in which a slowly varying ramped electric field is applied to the atoms. Measurements in which no HCPs are applied are interspersed at routine intervals during data acquisition to monitor the number of Rydberg atoms initially created and allow determination of the overall survival probability. The measured survival probabilities are large,  $\sim 90\%$  when  $\Delta p_A$  is small, demonstrating that the laser-excited atoms are efficiently transferred to the island. As  $\Delta p_A$  is increased, the survival probability decreases.

Selective loading is demonstrated by Figs. 3(a)–3(c), which correspond to three different values of the control parameters  $T_T$  and  $t_D$ . Those for Figs. 3(a) and 3(c) were chosen to place the wave packet on the shoreline of the main island but with initial  $z$  components of electron momentum of opposite sign (see Fig. 1). The ensuing variations in the average electron momentum  $\langle p_z \rangle$  are therefore  $\pi$  out of phase, which is reflected in the predicted and measured oscillations in the survival probability. The control parameters for Fig. 3(b) were selected to position the wave packet close to the center of the island. Little variation in  $\langle p_z \rangle$  is therefore expected and the oscillations in survival probability are greatly reduced.

Wave packet motion around the periphery of the main island also leads to periodic changes in electron energy (and  $n$ ). The evolution of the electron energy distribution, expressed in scaled units  $H_0^{\text{at}} = n_i^2 H^{\text{at}}$ , is shown in Fig. 4 for the same control parameters as utilized in Fig. 3. Strong periodic oscillations are seen in Figs. 4(a) and 4(c), which persist to large  $N$ . The widths of the energy variations ( $-0.7 < H_0^{\text{at}} < -0.45$  and  $-0.55 < H_0^{\text{at}} < -0.35$ ) are equal to the energy widths of the corresponding stable islands [Figs. 1(d) and 1(f)]. As expected, the energy fluctuations are minimal when the wave packet is placed in the center of the island [Fig. 4(b)]. The variations in the mean energy  $\langle H^{\text{at}} \rangle$  with  $N$  can be observed by probing the evolution of the wave packet after the train of pulses is turned off. The period of this evolution for a nonstationary wave packet is to leading order, given by the classical Kepler period  $T_{(n)} = 2\pi(-2\langle H^{\text{at}} \rangle)^{-3/2}$ , where  $\langle H^{\text{at}} \rangle$  depends on  $N$ . The period is monitored using a probe HCP applied at different time delays  $t_A$  after the HCP train.

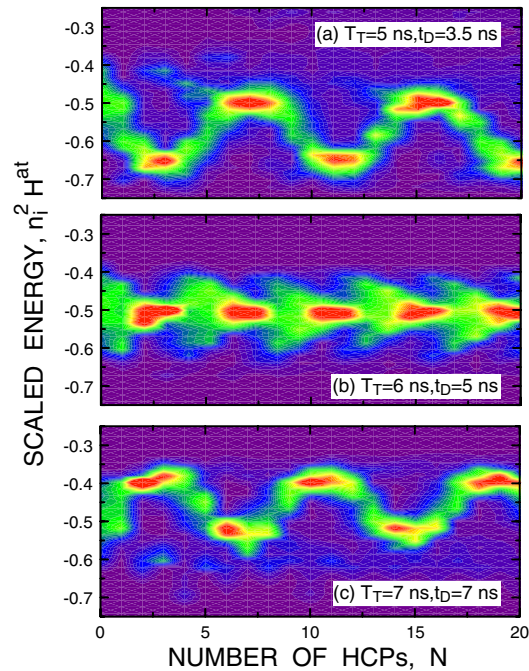


FIG. 4 (color online).  $N$  dependence of the calculated electron energy distribution for different values of  $T_T$  and  $t_D$  and initial wave packet placement at different locations on the periphery (a),(c) and at the center (b) of the island.

Typical experimental results are presented in Fig. 5. Periodic variations in survival probability are seen, the period changing from  $T_{\langle n \rangle} \sim 9.5$  ns for  $N = 3$  [Fig. 5(a)] to  $T_{\langle n \rangle} = 6.0$  ns for  $N = 8$  [Fig. 5(b)]. These periods are in good agreement with those predicted by CTMC simulations, although the predicted amplitudes of oscillation are somewhat larger than those measured, presumably as a

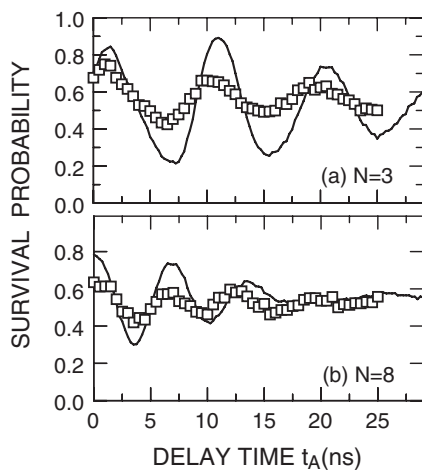


FIG. 5. Time evolution of the wave packet after  $N = 3$  and  $N = 8$  HCPs for  $T_T = 7$  ns and  $t_D = 7$  ns and a probe pulse of scaled strength  $\Delta p_{A_0} = 0.8$ . The experimental data (symbols) are compared with CTMC simulations (solid lines) that employ the same assumptions as for Fig. 3 (see text).

result of field inhomogeneities in the experiment and of uncertainties in the initial mix of Stark states excited.

The present work demonstrates the remarkable level of control over atomic wave packets that can be achieved in high Rydberg levels ( $n \gtrsim 350$ ). Using a carefully tailored sequence of HCPs we have successfully placed phase-space localized wave packets near the shore and near the center of a stable island and followed their subsequent motion within the island. Such time-resolved control over the position of the wave packet in combination with the suppression of its spread holds promise for realizing more complex protocols for steering wave packets to preselected regions of phase space or for switching population between islands. An interesting and open question is to what extent this level of control can be maintained over longer time scales (of the order of microseconds and beyond) when, on one hand, classical-quantum correspondence should begin to fail for fully coherent dynamics and, on the other hand, noise should induce decoherence and thus render the evolution “classical” after all.

This research is supported by the NSF under Grant No. PHYS-0353424 and by the Robert A. Welch Foundation. C. O. R. acknowledges support by the OBES, U.S. DOE to ORNL, which is managed by the UT-Battelle LLC under Contract No. DEPARTMENT-AC05-00OR22725. S. Y. and J. B. acknowledge support by the FWF-SFB016. J. C. L. acknowledges support from the ONR.

- [1] H. Maeda, D. Norum, and T. F. Gallagher, *Science* **307**, 1757 (2005); T. F. Gallagher, *Rydberg Atoms* (Cambridge University Press, New York, 1992).
- [2] J. Ahn, T. C. Weinacht, and P. H. Bucksbaum, *Science* **287**, 463 (2000).
- [3] F. B. Dunning, J. C. Lancaster, C. O. Reinhold, S. Yoshida, and J. Burgdörfer, *Adv. At. Mol. Phys.* **52**, 49 (2005).
- [4] W. Zhao, J. J. Mestayer, J. C. Lancaster, F. B. Dunning, C. O. Reinhold, S. Yoshida, and J. Burgdörfer, *Phys. Rev. Lett.* **95**, 163007 (2005).
- [5] R. R. Jones, D. You, and P. H. Bucksbaum, *Phys. Rev. Lett.* **70**, 1236 (1993); C. O. Reinhold, M. Melles, H. Shao, and J. Burgdörfer, *J. Phys. B* **26**, L659 (1993).
- [6] S. Yoshida, C. O. Reinhold, E. Persson, J. Burgdörfer, and F. B. Dunning, *J. Phys. B* **38**, S209 (2005).
- [7] A. Buchleitner, D. Delande, and J. Zakrzewski, *Phys. Rep.* **368**, 409 (2002).
- [8] W. Zhao, J. C. Lancaster, F. B. Dunning, C. O. Reinhold, and J. Burgdörfer, *Phys. Rev. A* **69**, 041401 (2004).
- [9] D. G. Arbó, C. O. Reinhold, J. Burgdörfer, A. K. Pattanyak, C. L. Stokely, W. Zhao, J. C. Lancaster, and F. B. Dunning, *Phys. Rev. A* **67**, 063401 (2003).
- [10] R. R. Jones, *Phys. Rev. Lett.* **76**, 3927 (1996).
- [11] C. O. Reinhold, J. Burgdörfer, M. T. Frey, and F. B. Dunning, *Phys. Rev.* **54**, R33 (1996).
- [12] C. L. Stokely, J. C. Lancaster, F. B. Dunning, D. G. Arbó, C. O. Reinhold, and J. Burgdörfer, *Phys. Rev. A* **67**, 013403 (2003).